

RESEARCH ARTICLE

10.1002/2016JA023666

Key Points:

- Asymmetric guide-field reconnection is observed at the magnetopause
- This reconnection is characterized by Hall pattern and Alfvénic plasma jet
- Symmetric Hall magnetic and electric fields were found in this event

Correspondence to:

H. S. Fu,
huishanf@gmail.com

Citation:

Peng, F. Z., et al. (2017), Quadrupolar pattern of the asymmetric guide-field reconnection, *J. Geophys. Res. Space Physics*, 122, 6349–6356, doi:10.1002/2016JA023666.

Received 6 NOV 2016

Accepted 6 JUN 2017

Accepted article online 9 JUN 2017

Published online 27 JUN 2017

Quadrupolar pattern of the asymmetric guide-field reconnection

F. Z. Peng¹, H. S. Fu¹, J. B. Cao¹, D. B. Graham², Z. Z. Chen¹, D. Cao¹, Y. Xu¹, S. Y. Huang³, T. Y. Wang¹, Y. V. Khotyaintsev², M. Andre², C. T. Russell⁴, B. Giles⁵, P.-A. Lindqvist⁶, R. B. Torbert⁷, R. E. Ergun⁸, and J. L. Burch⁹
¹School of Space and Environment, Beihang University, Beijing, China, ²Swedish Institute of Space Physics, Uppsala, Sweden, ³School of Electronic and Information, Wuhan University, Wuhan, China, ⁴Institute of Geophysics and Planetary Physics, University of California, Los Angeles, California, USA, ⁵NASA Goddard Space Flight Center, Greenbelt, Maryland, USA, ⁶Royal Institute of Technology, Stockholm, Sweden, ⁷Physics Department and Space Science Center, University of New Hampshire, Durham, New Hampshire, USA, ⁸Department of Astrophysical and Planetary Sciences, University of Colorado Boulder, Boulder, Colorado, USA, ⁹Southwest Research Institute, San Antonio, Texas, USA

Abstract With high-resolution data of the recently launched Magnetospheric Multiscale mission, we report a magnetic reconnection event at the dayside magnetopause. This reconnection event, having a density asymmetry $N_{\text{high}}/N_{\text{low}} \approx 2$ on the two sides of the reconnecting current sheet and a guide field $B_g \approx 0.4B_0$ in the “out-of-plane” direction, exhibit all the two-fluid features: Alfvénic plasma jets in the outflow region, bipolar Hall electric fields toward the current sheet center, quadrupolar Hall magnetic fields in the “out-of-plane” direction, and the corresponding Hall currents. Obviously, the density asymmetry $N_{\text{high}}/N_{\text{low}} \approx 2$ and the guide field $B_g \approx 0.4B_0$ are not sufficient to dismiss the quadrupolar pattern of Hall reconnection. This is different from previous simulations, where the bipolar pattern of Hall reconnection was suggested.

1. Introduction

Magnetic reconnection is a fundamental plasma process responsible for many explosive phenomena in the universe such as solar flares [Shibata et al., 1995], coronal mass ejection [Lin and Forbes, 2000], substorms [Angelopoulos et al., 2008], and the disruptions in laboratory plasmas [Ji et al., 1998]. During magnetic reconnection, the magnetic field topology changes and simultaneously the magnetic energy is converted into particles' kinetic and thermal energy [Priest and Forbes, 2000; Fu et al., 2015, 2017]. In the Earth's magnetosphere, such reconnection can occur at both the dayside magnetopause [e.g., Mozer et al., 2002; Dunlop et al., 2011; Lavraud et al., 2016; Burch et al., 2016; Cao et al., 2017] and nightside magnetotail [e.g., Øieroset et al., 2001; Eastwood et al., 2005; Wei et al., 2007; Fu et al., 2013a, 2013b; Cao et al., 2013; Zhou et al., 2014] and therefore provides an efficient approach for transferring solar wind energy into the Earth's magnetosphere [Dungey, 1961].

In order to understand the process of magnetic reconnection in space, many models have been proposed so far [Birn et al., 2001]. Among these models, the Hall reconnection model, or named two-fluid model, provides a very large energy-conversion rate during reconnection [Birn et al., 2001] and thus can interpret the explosive energy release reasonably. In space, particularly in the Earth's magnetosphere, such a Hall reconnection model has been widely accepted. The large reconnection rate in this model is attributed to the $j \times B$ term in the generalized Ohm's law. This term, $j \times B$, is prominent on the ion inertial scale (c/w_{pi}), meaning that Hall reconnection is actually a process occurring in the ion diffusion region. Here j is the current generated by the decoupled motion of the magnetized electrons and unmagnetized ions. Such a decoupled motion, on the ion inertial scale, certainly results in an electric field toward the current sheet center (Hall electric field), a current in the reconnection plane (Hall current), and an inductive magnetic field in the “out-of-plane” direction (Hall magnetic field). These structures have been verified using the spacecraft observations [e.g., Mozer et al., 2002; Eastwood et al., 2010b].

In the 2-D symmetric reconnection without guide field (e.g., the reconnection in the Earth's magnetotail), the Hall magnetic fields should be in a quadrupolar pattern [Dai et al., 2017]. In the asymmetric or guide-field reconnection (e.g., the reconnection at the Earth's magnetopause), however, the Hall magnetic fields tend to be in a bipolar pattern, according to previous simulations [e.g., Pritchett and Mozer, 2009;

Tanaka *et al.*, 2008; Huba, 2005]. In fact, observations of symmetric Hall pattern in the asymmetric reconnection without guide field have been reported at magnetopause [Teh *et al.*, 2010; Wang *et al.*, 2017]. Such influence of guide field and asymmetry on the Hall reconnection pattern has been summarized recently by Eastwood *et al.* [2013]. Typically, when the guide field and asymmetry increases, the symmetric Hall pattern inside the ion diffusion region gradually degenerates into an asymmetric pattern.

To improve our understanding of the Hall reconnection pattern, more spacecraft observations on the ion inertial scale are necessary. The Magnetospheric Multiscale (MMS) mission [Burch *et al.*, 2015], having an inter-spacecraft separation of ~ 10 km, provides a good opportunity to address this issue. In this paper, we report MMS observations of an asymmetric guide-field reconnection at the Earth's magnetopause. Differing from previous simulations, we find a clear quadrupolar pattern of Hall magnetic reconnection in this event.

2. Event Overview

The data from MMS mission [Burch *et al.*, 2015], particularly from the Fluxgate Magnetometers (FGM) [Russell *et al.*, 2016], Electric Double Probe [Lindqvist *et al.*, 2016; Torbert *et al.*, 2016], Axial Double Probe [Ergun *et al.*, 2016; Torbert *et al.*, 2016], and the Fast Plasma Instruments (FPI) [Pollock *et al.*, 2016] on board it, are used in this study. Throughout the paper, we use a local current sheet coordinate system (LMN) unless state otherwise. The establishment of this coordinate system will be introduced below.

The event we consider was detected on 3 December 2015, from 02:38:30 to 02:38:50 UT, when the four MMS spacecraft were located at (10.8, -2.3 , and -0.7) Earth radii (R_E) with a separation of ~ 15 km in geocentric solar ecliptic (GSE) coordinates. This separation is quite small, so that the four spacecraft generally measured similar magnetic field and plasma properties. For the purpose of simplicity, we show only the data from one of the spacecraft (MMS2) in this event.

Figures 1a–1c present an overview of this event from 02:32:00 to 02:42:00 UT, including the omnidirectional differential energy flux (dEF) of electrons (a), magnetic field in GSE coordinates (b), and the electron number density (c). Clearly, MMS2 crossed the magnetopause at 02:36:00 UT, when the electron dEF (Figure 1a) and density (Figure 1c) both increased significantly and the magnetic field strength decreased considerably (Figure 1b). From 02:36:00 to 02:38:40 UT, MMS2 situated well in the magnetopause boundary layer, as the overview shows the mixed properties of magnetosheath region after 02:39:00 UT (fluctuant fields, high number density, and soft electron spectrogram) and magnetosphere region before 02:36:00 UT (smooth fields, low number density, and hard electron spectrogram); it encountered a narrow current sheet at $\sim 02:38:40$ UT (see the shadow area). We particularly focus on this current sheet between magnetosheath (MSH) and magnetopause boundary layer in this study.

Figures 1d–1j are a close-up view of this current sheet from 02:38:30 to 02:38:50 UT. We see no clear change in B_x but a steep reversal of the direction of B_y and B_z during this period (Figure 1d). Such a reversal certainly means a narrow current sheet. We use the minimum variance analysis (MVA) to obtain the tangential direction of this current sheet (\mathbf{L}), i.e., the largest variation in the magnetic field. By using the timing method we could obtain the normal of the current sheet (\mathbf{N}) through the four satellites' time and location data of reversed B_L (magnetic fields in L direction) [Fu *et al.*, 2012, 2016]. The \mathbf{N} direction got here is nearly the same as the result of MVA. We cross \mathbf{N} and \mathbf{L} to get the \mathbf{M} direction and finally obtain the last direction as $\mathbf{N} = \mathbf{L} \times \mathbf{M}$. Obviously, (\mathbf{L} , \mathbf{M} , and \mathbf{N}) form an orthogonal coordinate system, in which the variation of magnetic field around the current sheet could be well described. With respect to the original GSE coordinates, $\mathbf{L} = (0.14 \ -0.73 \ 0.67)$, $\mathbf{M} = (0.14 \ 0.68 \ 0.72)$, and $\mathbf{N} = (-0.98 \ -0.01 \ 0.19)$.

We transfer the magnetic field and particle data from GSE to LMN coordinates. These data are shown in the right column of Figure 1, including the magnetic field strength $|B|$ (e), B_L (f), and B_M^* (g), B_N components (h), the electron flow velocity V_{eL} , V_{eM} , and V_{eN} (i), and the ion flow velocity V_{iL} , V_{iM} , and V_{iN} (j). In Figures 1e and 1g, the magnetic field in M direction is actually obtained after removal of the guide field, i.e., $B_M^* = B_M - 12.5$ nT. This guide field was determined by the mean value of magnetic field in M direction B_M (the Hall region should not be included). During this period, we see that the magnetic field B_L changes from $+35$ nT to -30 nT (Figure 1f), while the magnetic field B_N is generally stable and approaching zero (Figure 1h). The reversal of B_L direction happens at 02:38:40 UT (Figure 1f), when the magnetic field strength $|B|$, obtained after removal of the guide field, reaches its minimum (see Figure 1e). In principle, the current

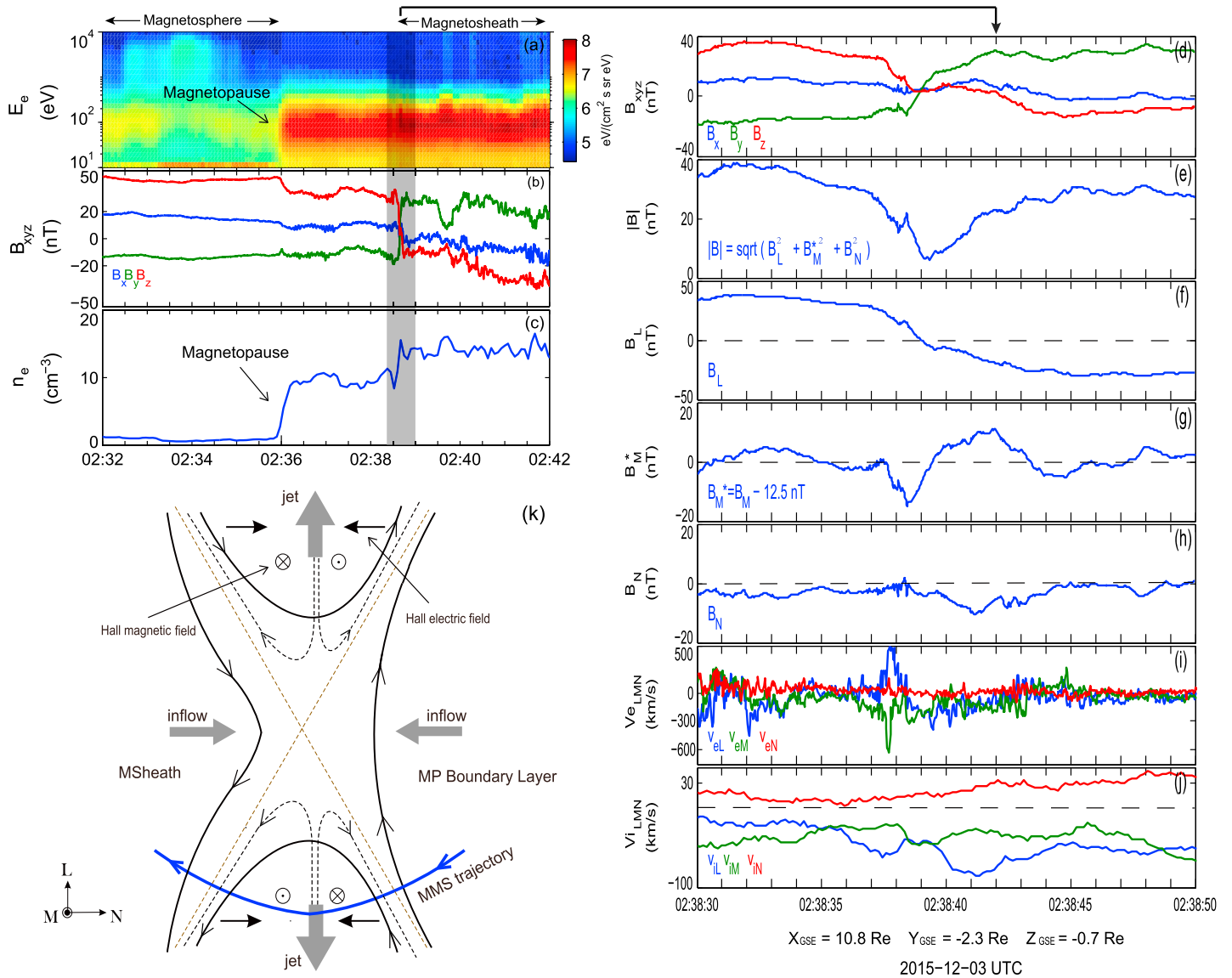


Figure 1. Overview of the reconnection event on 3 December 2015. (a) The omnidirectional differential energy fluxes of electrons. (b) The three components of magnetic field in GSE coordinates. (c) The electron number density. (d–j) A close-up view of the event from 02:38:30 to 02:38:50 UT. Specifically, the parameters are (Figure 1d) magnetic field B_x , B_y , and B_z components in GSE coordinates, (e) magnetic field strength with the guide field subtracted, (Figures 1f–1h) magnetic field B_L , B_M , and B_N components in LMN coordinates, and (Figures 1i and 1j) the electron and ion flow velocity. (k) A cartoon showing the asymmetric Hall reconnection at the Earth’s magnetopause. In Figure 1g, the guide field $B_g = 12.5$ nT has been subtracted. In Figure 1k, the blue thick line denotes the trajectory of MMS.

sheet center should be detected at $\sim 02:38:40$ UT associated with the minimum $|B|$ (Figure 1e). Around this current sheet, from 02:38:37 to 02:38:43.5 UT, we see a clear bipolar variation of magnetic field from $B_M^* \approx -15$ nT to $B_M^* \approx 12$ nT in M direction (Figure 1g) and a plasma jet $V_{iL} \approx 85$ km/s in L direction (Figure 1j). Such a bipolar variation is consistent with the Hall magnetic field in the two-fluid model. Also, the plasma jet has a velocity comparable to the inflow Alfvén speed $VA = \sqrt{\frac{B_1 B_2 (B_1 + B_2)}{\mu_0 (\rho_1 B_1 + \rho_2 B_2)}} \sim 120$ km/s, where B_1 , B_2 and ρ_1 , ρ_2 are respectively the reconnecting fields and mass densities on the two sides of current sheet [Cassak and Shay, 2007]. These two characteristics (bipolar magnetic field and Alfvénic jet) around the current sheet indicate that the region MMS2 crossed during 02:38:37–02:38:43.5 UT may be the ion diffusion region of magnetic reconnection. Such ion diffusion region has been reported previously in the Earth’s magnetosphere and the magnetosheath [Mozer et al., 2002; Eastwood et al., 2010b; Retino et al., 2007]. We illustrate the crossing the ion diffusion region in this event in Figure 1k, where the thick blue line denotes the spacecraft trajectory. Considering the number density asymmetry (Figure 2a) and also the

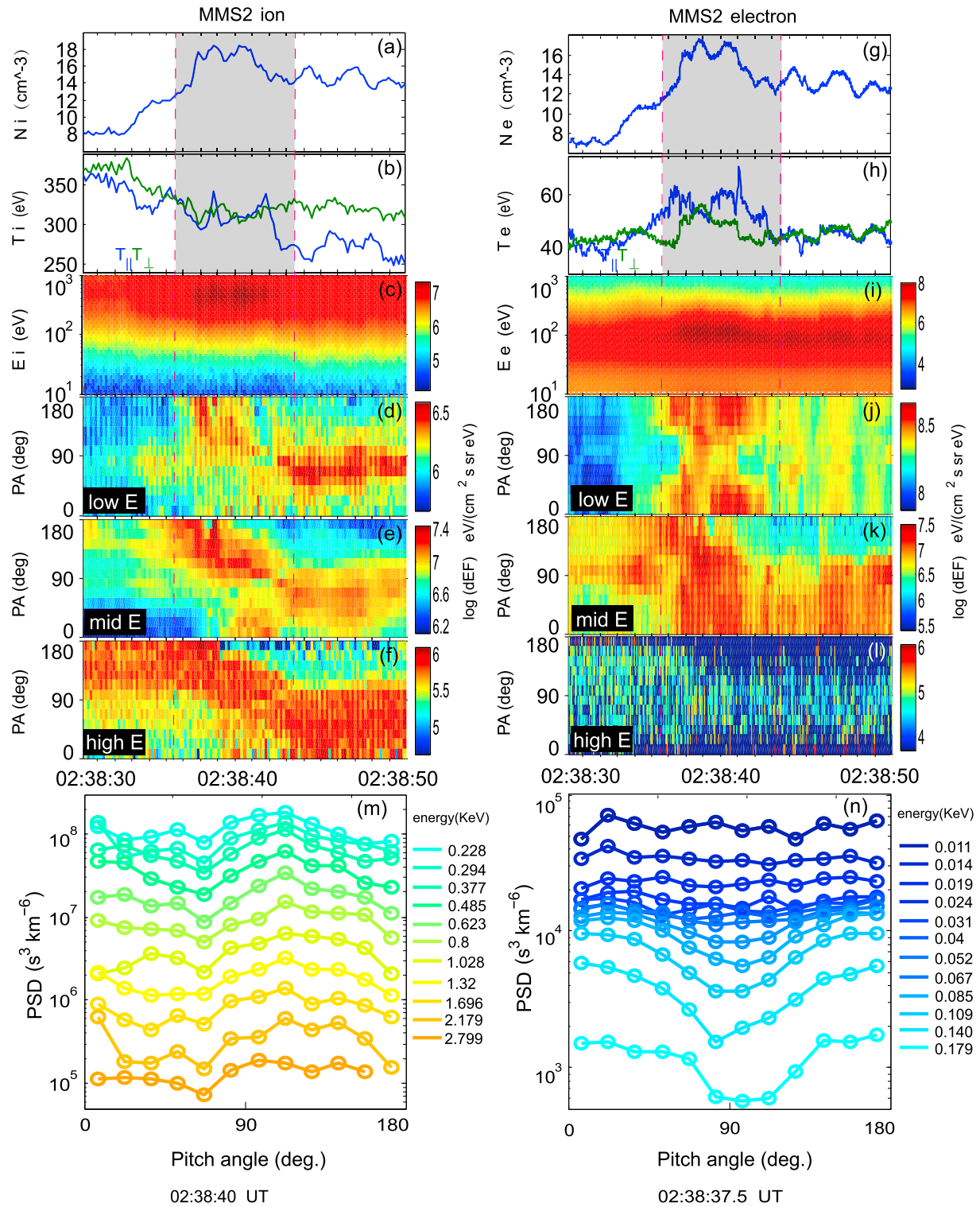


Figure 2. Plasma properties and detailed pitch angle distributions of ions (left column) and electrons (right column) measured by MMS2. (a, g) The number density. (b, h) The parallel (blue) and perpendicular (red) temperature. (c, i) The omnidirectional differential energy fluxes of the 0.01–1 keV ions and electrons. (d–f, j–l) Pitch angle distribution of the low-energy (0.02–0.2 keV), middle-energy (0.2–3 keV), and high-energy (3–30 keV) particles. (m) Detailed pitch angle distributions of ions at 02:38:40 UT for 11 different channels from 0.228 keV to 2.799 keV (middle-energy). (n) Detailed pitch angle distributions of electrons at 02:38:37.5 UT for 12 different channels from 0.011 keV to 0.179 keV (low-energy).

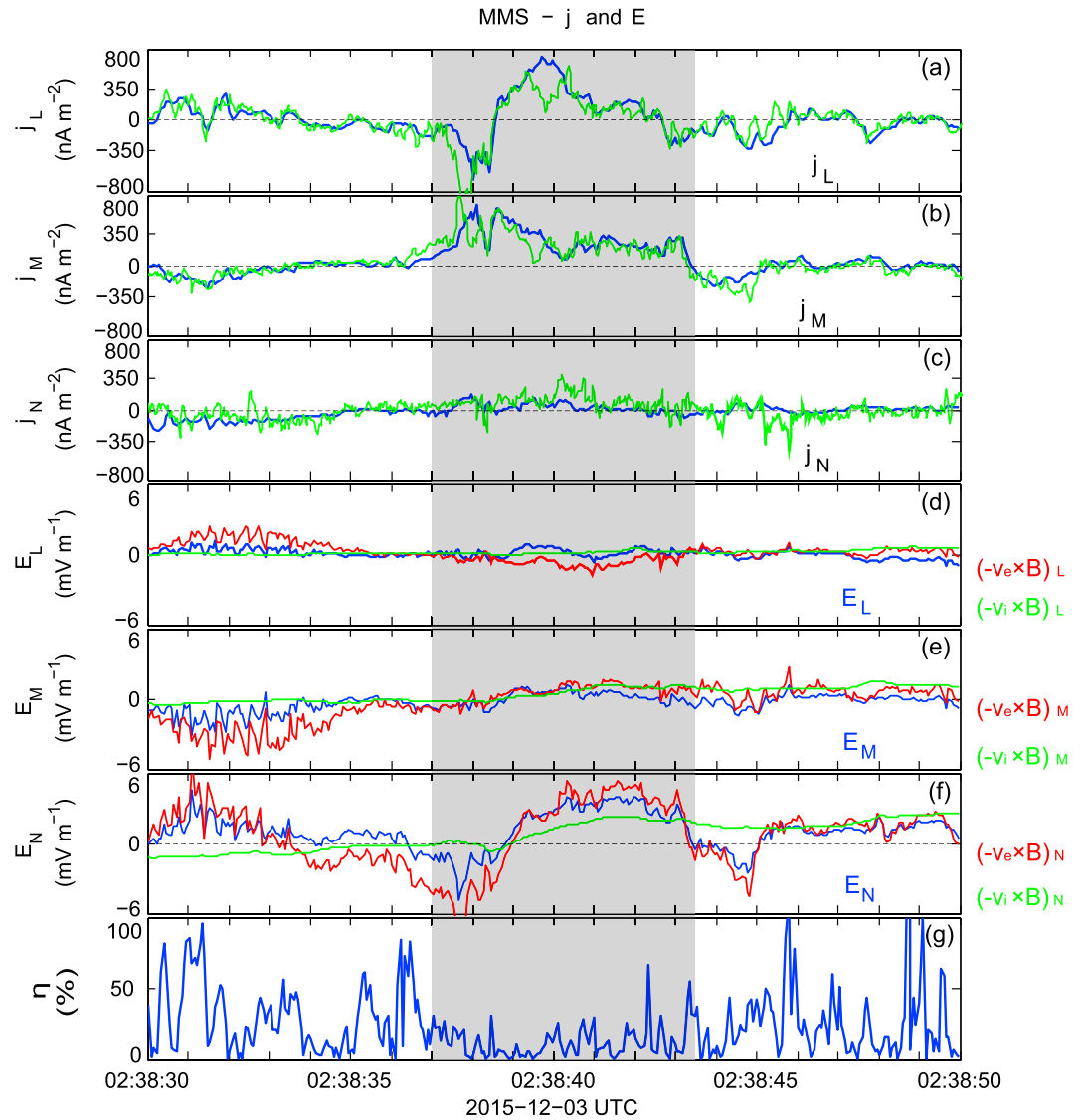


Figure 3. The electric field and current system detected by MMS from 02:38:30 to 02:38:50 UT. (a–c) The three components of current density in LMN coordinates, with the blue line representing the result from Curlometer [Dunlop et al., 2002] while the green line the result from plasma moments. (d–f) The measurements of electric field (blue line), electron convection term $-V_e \times B$ (red line), and ion convection term $-V_i \times B$ (green) in the LMN coordinate system. (g) The parameter η , for estimating the error of Curlometer.

strong guide field during the whole crossing ($B_g = 12.5$ nT, see Figure 1g), the magnetic reconnection observed in this event should be an asymmetric guide-field Hall reconnection. The bipolar variation of the Hall electric field, formed due to the separated motion of electrons and ions on ion inertial scale, is also found in this event (see Figure 3). At 02:38:37.5 UT, a strong electron flow was detected (Figure 1i), probably at the separatrix of the ion diffusion region.

The bipolar variation of magnetic field in the “out-of-plane” direction (M direction), traditionally interpreted as the Hall quadrupolar magnetic field, is clearly seen in this event. Such phenomenon is unusual in the asymmetric guide-field reconnection [Eastwood et al., 2013]. We will discuss it in detail in section 5.

3. Plasma Properties

Figure 2 shows the plasma properties of ions (left column) and electrons (right column) in this asymmetric guide-field reconnection, measured by MMS2 from 02:38:30 to 02:38:50 UT. Specifically, the plasma density

(a, g), temperature (b, h), omnidirectional dEF of the 0.01–1 keV particles (c, i), pitch angle distribution (PAD) of the 0.02–0.2 keV (d, j), 0.2–3 keV (e, k), and 3–30 keV particles (f, l) are shown from top to bottom. We find that the plasma density on the Earth side of the current sheet (02:38:30–02:38:35 UT), $N_i = 8 \text{ cm}^{-3}$, is clearly smaller than that on the Sun side of the current sheet (02:38:43–02:38:50 UT), $N_i = 16 \text{ cm}^{-3}$. Such density discrepancy on the two sides of the current sheet, as shown in Figures 2a and 2g, confirms that the reconnection is asymmetric.

During the whole crossing (02:38:30–02:38:50 UT), the ion temperature is generally positive anisotropic ($T_{\perp} > T_{\parallel}$) (see Figure 2b) while the electron temperature is nearly isotropic ($T_{\parallel} \approx T_{\perp}$) (see Figure 2h). This is different from that inside the ion diffusion region (02:38:37–02:38:43.5 UT), where the electron temperature shows the signature of " $T_{\parallel} > T_{\perp}$ " (see Figure 2h) and the ion temperature is isotropic (Figure 2b) (see the shadow area). We see an enhancement of the number density of ions and electrons inside the ion diffusion region (Figures 2a and 2g). Such enhancement is primarily contributed from the 0.1–1 keV ions (Figure 2c) and 0.04–0.4 keV electrons (Figure 2i), i.e., the middle-energy ions and low-energy electrons according to the classification of FPI [Pollock *et al.*, 2016]. Inside the ion diffusion region, the fluxes of these middle-energy ions between pitch angle 90° and 180° are generally higher than that of 0° to 90° (Figures 2e and 2m), while the PADs of the low-energy electrons are "cigar-type" (Figures 2j and 2n), consistent with the estimation of plasma temperature (Figures 2b and 2h). Comparing to the dEFs of the low-energy electrons (Figure 2j), the dEFs of the high-energy electrons are significantly lower (Figure 2l), meaning that there is no electron energization in this event.

4. Electric Field and Current System

Figure 3 investigates the electric field and current system inside the ion diffusion region. From top to bottom, the current density j_L , j_M , and j_N (a–c), the electric field E_L , E_M , and E_N (d–f), and the parameter $\eta \equiv |\nabla \cdot \mathbf{B}| / |\nabla \times \mathbf{B}|$ (g) are shown, respectively. In Figures 3a–3c, the blue line represents the current density derived from the curlometer method [Dunlop *et al.*, 2002], while the green line denotes the current density from the plasma moments $\mathbf{j} = n \cdot \mathbf{e} \cdot (\mathbf{V}_i - \mathbf{V}_e)$. In Figures 3d–3f, the blue, red, and green lines show the measurements of electric field \mathbf{E} , the convection term $-\mathbf{V}_e \times \mathbf{B}$ and $-\mathbf{V}_i \times \mathbf{B}$, respectively. Here \mathbf{V}_i , \mathbf{V}_e , \mathbf{E} , and \mathbf{B} are the average of the four-spacecraft measurements; n is the average of the ion and electron density, $n = (n_i + n_e)/2$.

As can be seen, the current densities derived from these two methods are quite similar. Outside the ion diffusion region, all the current components (j_L , j_M , and j_N) are nearly zero (Figures 3a–3c); while inside the diffusion region (see the shadow area), we find a clear enhancement of current in M direction (Figure 3b) and a "negative-positive-negative" variation of current in L direction (Figure 3a). Obviously, the large j_M can be interpreted as the "out-of-plane" current of the current sheet (similar to the cross-tail current in magnetotail or the Chapman-Ferraro current at magnetopause), while the "negative-positive-negative" variation of j_L may be interpreted as the Hall current inside the ion diffusion region. Such interpretation is well consistent with that shown in Figure 1k (see particularly the black dashed lines there). The most prominent fluctuation of electric field is found in the E_N component (Figure 3f). Roughly speaking, the measurements of electric field (Figures 3d–3f, blue line) during 02:38:37–02:38:43.5 UT are consistent with the electron convection term $-\mathbf{V}_e \times \mathbf{B}$ (Figures 3d–3f, red line) but different from the ion convection term $-\mathbf{V}_i \times \mathbf{B}$ (Figures 3d–3f, green line) and thus confirm the identification of ion diffusion region. We see a "negative-positive" variation of E_N inside the ion diffusion region (see the shadow area). Such a bipolar variation may be interpreted as the symmetric bipolar Hall electric field (see the black thick arrows in Figure 1k).

5. Summary and Discussion

On 3 December 2015, MMS crossed a narrow current sheet at the dayside magnetopause with separation of ~ 15 km. It detected all the signatures of Hall magnetic reconnection from 02:38:30 to 02:38:50 UT, including the Alfvénic plasma jets, bipolar Hall electric fields, quadrupolar Hall magnetic fields, and the corresponding Hall currents, and therefore, it may encountered the ion diffusion region of a Hall magnetic reconnection. Inside this ion diffusion region, we find that ions are demagnetized ($\mathbf{E} \neq -\mathbf{V}_i \times \mathbf{B}$) while electrons are generally frozen-in ($\mathbf{E} \approx -\mathbf{V}_e \times \mathbf{B}$). As a result, the middle-energy electrons show an isotropic pitch angle distribution

inside the diffusion region, while the low-energy electrons exhibit a cigar-type PAD inside the diffusion region. We find no clear electron energization inside the ion diffusion region.

During the encounter of this event, MMS observed a guide field in the M direction, i.e., the “out-of-plane” direction. This guide field, $B_g = 12.5$ nT, is approximately 40% of the reconnecting field ($B_g = 0.4B_0$). On the two sides of the reconnection current sheet, the plasma density and magnetic field are both asymmetric. Specifically, the plasma density on the Earth side of the current sheet ($N_i = 8 \text{ cm}^{-3}$) is about 50% of the plasma density on the Sun side ($N_i = 16 \text{ cm}^{-3}$) (see Figure 2a), while the magnetic field strength on the Earth side ($|B_L| = 35$ nT) is about 120% of the magnetic field strength on the Sun side ($|B_L| = 30$ nT) (see Figure 1f). All these parameters indicate that the reconnection detected by MMS in this event is an asymmetric guide-field Hall reconnection. In fact, the MMS spacecraft spent ~ 2 s to cross the Earth side of the ion diffusion region (02:38:37.5–02:38:39.5 UT) but ~ 4 s to cross the Sun side of the diffusion region (02:38:39.5–02:38:43.5 UT) (see Figure 1g). This is consistent with the identification of the asymmetric guide-field reconnection.

In the asymmetric guide-field reconnection, the quadrupolar Hall magnetic field and bipolar Hall electric field are supposed to degenerate into asymmetric pattern, according to previous simulations [e.g., Pritchett and Mozer, 2009; Tanaka et al., 2008]. Specifically, the Hall magnetic field on one side of the current sheet, where the magnetic field is stronger and the plasma density is lower (with respect to those on another side), will disappear due to the electron flows along separatrices from high-density side to low-density side of the current sheet [Pritchett and Mozer, 2009]. And the guide field may further destroy the symmetric scale pattern of Hall electric fields and magnetic fields, by exerting a $\mathbf{j}_{\text{Hall}} \times \mathbf{B}_g$ force on the ion diffusion region [Eastwood et al., 2010a; Rogers et al., 2003]. Also, a moderate guide field alone could lead to the large asymmetry of the quadrupolar Hall magnetic field, and the Hall magnetic field in positive N direction will decrease, while the guide field in M direction is getting bigger gradually (the N and M direction used here are consistent with Figure 1k) [Huba, 2005]. In the present event, both guide field (Figure 1g) and asymmetric plasma density (Figure 2a) exist, but the symmetric pattern of Hall electric field and magnetic field is still found (Figures 1g and 3f). Obviously, the asymmetry of reconnection and the guide field do not significantly affect the quadrupolar pattern of Hall reconnection in this event (However, the Hall magnetic field on the low-density side ($B_M^* \approx -15$ nT) is even stronger than that on the high-density side ($B_M^* \approx 12$ nT); see Figure 1g). This is different from previous simulations, which predict bipolar pattern in the asymmetric guide-field reconnection [see Eastwood et al., 2013, and references therein].

The discrepancy between our observations and previous simulations may be attributed to the small values of guide field and asymmetry in this event. Probably, the guide field $B_g = 0.4B_0$ and density ratio $N_{\text{high}}/N_{\text{low}} \approx 2$ are not sufficient to completely destroy the quadrupolar pattern of Hall reconnection. To validate this conjecture, however, a quantitative test in the simulations is necessary. Besides, the scale of Hall magnetic field on the low-density side (~ 2 s duration, see Figure 1g) is about one half of the scale of Hall magnetic field on the high-density side (~ 4 s duration, see Figure 1g). This is quantitatively consistent with the density asymmetry $N_{\text{high}}/N_{\text{low}} \approx 2$ on the two sides. Such consistence should also be tested quantitatively in the future simulations. Another explanation to our observation is that may be the number density asymmetry and guide field are competing with each other in this event, which makes the symmetric pattern of Hall fields still exists. And the mechanism of this could be studied in future works.

Acknowledgments

We thank the MMS Science Data Center (<https://lasp.colorado.edu/mms/sdc/public/>) for providing the data for this study. This research was supported by NSFC grants 41574153, 41431071, and 41404133, and the ISSI travel grant for team “MMS and Cluster Observations of Magnetic Reconnection.”

References

- Angelopoulos, V., et al. (2008), Tail reconnection triggering substorm onset, *Science*, 321, 931–935, doi:10.1126/science.1160495.
- Birn, J., et al. (2001), Geospace Environmental Modeling (GEM) magnetic reconnection challenge, *J. Geophys. Res.*, 106, 3715–3720, doi:10.1029/1999JA900449.
- Burch, J. L., T. E. Moore, R. B. Torbert, and B. L. Giles (2015), Magnetospheric Multiscale overview and science objectives, *Space Sci. Rev.*, doi:10.1007/s11214-015-0164-9.
- Burch, J. L., et al. (2016), Electron-scale measurements of magnetic reconnection in space, *Science*, doi:10.1126/science.aaf2939.
- Cao, J. B., X. H. Wei, A. Y. Duan, H. S. Fu, T. L. Zhang, H. Reme, and I. Dandouras (2013), Slow magnetosonic waves detected in reconnection diffusion region in the Earth’s magnetotail, *J. Geophys. Res. Space Physics*, 118, 1659–1666, doi:10.1002/jgra.50246.SCI.
- Cao, D., et al. (2017), MMS observations of whistler waves in electron diffusion region, *Geophys. Res. Lett.*, 44, 3954–3962, doi:10.1002/2017GL072703.
- Cassak, P. A., and M. A. Shay (2007), Scaling of asymmetric magnetic reconnection: General theory and collisional simulations, *Phys. Plasmas*, 14, 102114, doi:10.1063/1.2795630.
- Dai, L., C. Wang, Y. Zhang, B. Lavraud, J. Burch, C. Pollock, and R. B. Torbert (2017), Kinetic Alfvén wave explanation of the Hall fields in magnetic reconnection, *Geophys. Res. Lett.*, 44, 634–640, doi:10.1002/2016GL071044.

- Dungey, J. W. (1961), Interplanetary magnetic field and the auroral zones, *Phys. Rev. Lett.*, *6*, 47–48, doi:10.1103/PhysRevLett.6.47.
- Dunlop, M. W., A. Balogh, K.-H. Glassmeier, and P. Robert (2002), Four-point Cluster application of magnetic field analysis tools: The Curlometer, *J. Geophys. Res.*, *107*(A11), 1384, doi:10.1029/2001JA005088.
- Dunlop, M. W., et al. (2011), Extended magnetic reconnection across the dayside magnetopause, *Phys. Rev. Lett.*, *107*, 025004, doi:10.1103/PhysRevLett.107.025004.
- Eastwood, J. P., D. G. Sibeck, J. A. Slavin, M. L. Goldstein, B. Lavraud, M. Sitnov, S. Imber, A. Balogh, E. A. Lucek, and I. Dandouras (2005), Observations of multiple X-line structure in the Earth's magnetotail current sheet: A Cluster case study, *Geophys. Res. Lett.*, *32*, L11105, doi:10.1029/2005GL022509.
- Eastwood, J. P., M. A. Shay, T. D. Phan, and M. Øieroset (2010a), Asymmetry of the ion diffusion region Hall electric and magnetic fields during guide field reconnection: Observations and comparison with simulations, *Phys. Rev. Lett.*, *104*(20), 205501, doi:10.1103/PhysRevLett.104.205001.
- Eastwood, J. P., T. D. Phan, M. Øieroset, and M. A. Shay (2010b), Average properties of the magnetic reconnection ion diffusion region in the Earth's magnetotail: 2001–2005 Cluster observations and comparison with simulations, *J. Geophys. Res.*, *115*, A08215, doi:10.1029/2009JA014962.
- Eastwood, J. P., T. D. Phan, M. Øieroset, M. A. Shay, K. Malakit, M. Swisdak, J. F. Drake, and A. Masters (2013), Influence of asymmetries and guide fields on the magnetic reconnection diffusion region in collisionless space plasmas, *Plasma Phys. Controlled Fusion*, *55*, 124001, doi:10.1088/0741-3335/55/12/124001.
- Ergun, R. E., et al. (2016), The axial double probe and fields signal processing for the MMS mission, *Space Sci. Rev.*, *199*(1), 167–188, doi:10.1007/s11214-014-0115-x.
- Fu, H. S., Y. V. Khotyaintsev, A. Vaivads, M. André, and S. Y. Huang (2012), Electric structure of dipolarization front at sub-proton scale, *Geophys. Res. Lett.*, *39*, L06105, doi:10.1029/2012GL051274.
- Fu, H. S., et al. (2013a), Dipolarization fronts as a consequence of transient reconnection: In situ evidence, *Geophys. Res. Lett.*, *40*, 6023–6027, doi:10.1002/2013GL058620.
- Fu, H. S., Y. V. Khotyaintsev, A. Vaivads, A. Retinò, and M. André (2013b), Energetic electron acceleration by unsteady magnetic reconnection, *Nat. Phys.*, *9*, 426–430, doi:10.1038/nphys2664.
- Fu, H. S., A. Vaivads, Y. V. Khotyaintsev, V. Olshevsky, M. André, J. B. Cao, S. Y. Huang, A. Retinò, and G. Lapenta (2015), How to find magnetic nulls and reconstruct field topology with MMS data?, *J. Geophys. Res. Space Physics*, *120*, 3758–3782, doi:10.1002/2015JA021082.
- Fu, H. S., et al. (2016), Identifying magnetic reconnection events using the FOTE method, *J. Geophys. Res. Space Physics*, *121*, 1263–1272, doi:10.1002/2015JA021701.
- Fu, H. S., A. Vaivads, Y. V. Khotyaintsev, M. André, J. B. Cao, V. Olshevsky, J. P. Eastwood, and A. Retinò (2017), Intermittent energy dissipation by turbulent reconnection, *Geophys. Res. Lett.*, *44*, 37–43, doi:10.1002/2016GL071787.
- Huba, J. D. (2005), Hall magnetic reconnection: Guide field dependence, *Phys. Plasmas*, *12*, 012322.
- Ji, H., M. Yamada, S. Hsu, and R. Kulsrud (1998), Experimental test of the Sweet-Parker model of magnetic reconnection, *Phys. Rev. Lett.*, *30*, 3256.
- Lavraud, B., et al. (2016), Currents and associated electron scattering and bouncing near the diffusion region at Earth's magnetopause, *Geophys. Res. Lett.*, *43*, 3042–3050, doi:10.1002/2016GL068359.
- Lin, J., and T. G. Forbes (2000), Effects of reconnection on the coronal mass ejection, *J. Geophys. Res.*, *105*(A2), 2375–2392, doi:10.1029/1999JA000477.
- Lindqvist, P.-A., et al. (2016), The spin-plane double probe instruments for MMS, *Space Sci. Rev.*, *199*, 137–165, doi:10.1007/s11214-014-0116-9.
- Mozer, F. S., S. D. Bale, and T. D. Phan (2002), Evidence of diffusion regions at a subsolar magnetopause crossing, *Phys. Rev. Lett.*, *89*, 015002.
- Øieroset, M., T. Phan, M. Fujimoto, R. Lin, and R. Lepping (2001), In situ detection of collisionless reconnection in the Earth's magnetotail, *Nature*, *412*, 414–417.
- Pollock, C., et al. (2016), Fast plasma investigation for magnetospheric multiscale, *Space Sci. Rev.*, doi:10.1007/s11214-016-0245-4.
- Priest, E., and T. Forbes (2000), *Magnetic Reconnection: MHD Theory and Applications*, pp. 1–45, Cambridge Univ. Press, Cambridge, U. K.
- Pritchett, P. L., and F. S. Mozer (2009), Asymmetric magnetic reconnection in the presence of a guide field, *J. Geophys. Res.*, *114*, A11210, doi:10.1029/2009JA014343.
- Retino, A., D. Sundkvist, A. Vaivads, F. Mozer, M. Andre, and C. J. Owen (2007), In situ evidence of magnetic reconnection in turbulent plasma, *Nat. Phys.*, *3*, 236–238.
- Rogers, B. N., R. E. Denton, and J. F. Drake (2003), Signatures of collisionless magnetic reconnection, *J. Geophys. Res.*, *108*(A3), 1111, doi:10.1029/2002JA009699.
- Russell, C. T., et al. (2016), The Magnetospheric Multiscale magnetometers, *Space Sci. Rev.*, *199*, 189–256, doi:10.1007/s11214-014-0057-3.
- Shibata, K., et al. (1995), Hot-plasma ejections associated with compact-loop solar flares, *Astrophys. J.*, *451*, L83–L85.
- Tanaka, K. G., et al. (2008), Effects on magnetic reconnection of a density asymmetry across the current sheet, *Ann. Geophys.*, *26*, 2471.
- Teh, W. L., S. E. B. U. O. Sonnerup, R. Ergun, V. Angelopoulos, K.-H. Glassmeier, J. P. McFadden, and J. W. Bonnell (2010), THEMIS observations of a secondary magnetic island within the hall electromagnetic field region at the magnetopause, *Geophys. Res. Lett.*, *37*, L21102, doi:10.1029/2010GL045056.
- Torbert, R. B., et al. (2016), The FIELDS instrument suite on MMS: Scientific objectives, measurements, and data products, *Space Sci. Rev.*, *199*, 105–135, doi:10.1007/s11214-014-0109-8.
- Wang, R., et al. (2017), Electron-scale quadrants of the Hall magnetic field observed by the Magnetospheric Multiscale spacecraft during asymmetric reconnection, *Phys. Rev. Lett.*, *118*, 175101.
- Wei, X. H., J. B. Cao, G. C. Zhou, O. Santolík, H. Rème, I. Dandouras, N. Cornilleau-Wehrlin, E. Lucek, C. M. Carr, and A. Fazakerley (2007), Cluster observations of waves in the whistler frequency range associated with magnetic reconnection in the Earth's magnetotail, *J. Geophys. Res.*, *112*, A10225, doi:10.1029/2006JA011771.
- Zhou, M., H. Li, X. Deng, S. Huang, Y. Pang, Z. Yuan, X. Xu, and R. Tang (2014), Characteristic distribution and possible roles of waves around the lower hybrid frequency in the magnetotail reconnection region, *J. Geophys. Res. Space Physics*, *119*, 8228–8242, doi:10.1002/2014JA019978.